Phenomenological modelling of damage in polymer blends

PHENOMENOLOGICAL MODELLING OF DAMAGE IN POLYMER BLENDS

P.H.M. TIMMERMANS, W.A.M. BREKELMANS and J.H.P. DE VREE

Faculty of Mechanical Engineering,
Eindhoven University of Technology, The Netherlands

Summary

To describe the constitutive behaviour of a certain class of polymer blends an elasto-perfectly-viscoplastic and creep damageable material characterization is proposed. For a composite of 80 % Polystyrene and 20 % Ethylene Propylene Diene Monomer rubber (PS/EPDM) the specific parameters are determined from tensile tests in a particular range of strain velocities. To investigate the applicability of the model, the results of a finite element analysis for a laterally loaded thin plate (plane stress) with a circular hole are compared to measurements. Numerically calculated values are in reasonable agreement with reality; discrepancies can be ascribed to noise in experimental data. The finite element approach is evaluated with respect to the occurrence of mesh-dependence. Mesh-refinement shows convergence of solutions, attributable to the stabilizing influence of the viscous contribution in the constitutive equations.

1. Introduction

Theories in Continuum Damage Mechanics (Kachanov, 1986; Lemaitre and Chaboche, 1990) are conceptually based on the introduction of a continuously distributed internal state variable, the damage D, representative for the local degeneration of the material due to the initiation and development of micro-defects (micro-cracks and voids). In this paper the constitutive equations for elasto-perfectly-viscoplastic material, extended by a damage contribution (Marquis, 1989), are adopted. It is the objective of the present research to evaluate the performance of such an enriched formulation for the modelling of the mechanical behaviour of polymer blends. It is assumed that the damage is isotropic, consequently D is a scalar variable. Thermal effects are left out of consideration.

From the variety of polymer blends a typical composite has been selected: a mixture of 80 % Polystyrene and 20 % Ethylene Propylene Diene Monomer rubber. This material combines a number of properties, appropriate for the actual approach. The salient strain rate dependence justifies a viscous modelling, small strains until failure allow for a geometrically linear analysis, the absence of strain localization in uniaxial tests facilitates the determination of the material parameters.

In section 2 of this paper the fundamental constitutive equations are considered. A comparative confrontation of the one-dimensional version of the theory with tensile test data (in a sufficient broad range of strain rates) leads to an estimation of material

J.F. Dijksman and F.T.M. Nieuwstadt (eds.), Topics in Applied Mechanics, 147–154.

parameters. Section 3 discusses the verification experiment. A thin rectangular plate with a circular hole is loaded in a tensile testing machine. The relative velocity of two opposite sides is prescribed. The positions of a set of markers on the plate are recorded by the Hentschel-system (Zamzow, 1990), a camera continuously tracking the markers supplies the co-ordinates of a discrete number of material points of the plate in dependence on time. From the marker positions the strain fields (and the strain rates) can be derived.

For the numerical simulations of arbitrary configurations the finite element method is most suitable. In section 4 attention is focussed on the implementation of the constitutive equations and some computational details. In section 5 the numerical results are compared to measurements. Moreover, the effect of mesh-refinement is examined. Section 6 presents the conclusions.

2. Theoretical derivation of the constitutive equations

Strain-softening (negative tangential stiffness) in rate-independent plasticity causes the loss of ellipticity of the system of equations in continuum mechanics. Solutions of these equations show spurious localization of deformation. By regularization of the dissipation function (Simo, 1988) the loss of ellipticity is prevented and simulations remain physically meaningful (Needleman, 1988). The adaptation leads to the classical viscoplastic formulation, adequate to model the material behaviour under consideration in this paper; the softening originates from damage evolution. In this section the regularization is reviewed to derive the constitutive description. One-dimensional response experiments enable the quantification of the model.

2.1 Regularization of the dissipation function

The constitutive formulation for elasto-perfectly-plastic material behaviour (no hardening effects) is taken as point of departure. Helmholtz free energy potential ψ (per unit of volume) can be written as

$$\psi = \frac{1}{2}(\boldsymbol{\varepsilon} - \boldsymbol{\varepsilon}^p) : {}^4\boldsymbol{H} : (\boldsymbol{\varepsilon} - \boldsymbol{\varepsilon}^p) \tag{2.1}$$

with $\boldsymbol{\varepsilon}$ the total linear strain tensor, $\boldsymbol{\varepsilon}^p$ the plastic part of the total strain (to be considered as internal state variable) and with ${}^4\boldsymbol{H}$ the material stiffness tensor of rank four according to (E: Young's modulus, ν: Poisson's ratio):

$${}^4\boldsymbol{H} = \frac{E}{1+\nu}\left({}^4\boldsymbol{I} + \frac{\nu}{1-2\nu}\boldsymbol{II}\right) \tag{2.2}$$

The Cauchy stress tensor $\boldsymbol{\sigma}$ can be obtained from

$$\boldsymbol{\sigma} = \frac{\partial \psi}{\partial \boldsymbol{\varepsilon}} = {}^4\boldsymbol{H} : (\boldsymbol{\varepsilon} - \boldsymbol{\varepsilon}^p) \tag{2.3}$$

while the dissipation function D^p (Simo, 1988) is defined by

$$D^p = -\frac{\partial \psi}{\partial \boldsymbol{\varepsilon}^p} : \dot{\boldsymbol{\varepsilon}}^p = \boldsymbol{\sigma} : \dot{\boldsymbol{\varepsilon}}^p \tag{2.4}$$

The stress tensor $\boldsymbol{\sigma}$ should satisfy the yield criterion (von Mises), according to

$$\Phi(\sigma) = J(s) - \kappa \leq 0 \quad ; \quad J(s) = \sqrt{\frac{3}{2} s:s} \quad ; \quad s = \sigma - \frac{1}{3} tr(\sigma) I \tag{2.5}$$

where $J(s)$ represents the equivalent stress, s the stress deviator, I the identity tensor and κ the yield stress. The total strain rate has a plastic component only if $\Phi(\sigma)=0$.

The "direction" of the plastic strain rate tensor, perpendicular on the representation of the plastic potential (to be specified) in the stress domain, is prescribed by the flow rule. This completes the constitutive description for elasto-perfectly-plastic behaviour. The flow rule is called associative if the plastic potential is equivalent to $\Phi(\sigma)$.

The associative flow rule can alternatively be formulated by the principle of maximum dissipation:

$$\sigma : \dot{\varepsilon}^p = \max_{\Phi(\tau) \leq 0} \{\tau : \dot{\varepsilon}^p\} \tag{2.6}$$

This principle states that for a given plastic strain rate $\dot{\varepsilon}^p$, among all admissible stresses τ satisfying the yield criterion, the dissipation function D^p attains its maximum value for the actual stress σ. By approximation, the condition $\Phi(\tau) \leq 0$ can be taken into account by extension of D^p with a penalty contribution, leading to the definition of the regularized dissipation function D_η^p as

$$D_\eta^p = \sigma : \dot{\varepsilon}^p - \frac{1}{\eta} \frac{1}{n+1} \langle \Phi(\sigma) \rangle^{n+1} \tag{2.7}$$

where $\langle x \rangle = (x + |x|)/2$ denotes the ramp function and with η and n positive penalty parameters, however, in the following to be considered as material properties. The above choice for the penalty term simplifies further elaborations. Unconstrained maximization of the expression (2.7) with respect to σ results in

$$\dot{\varepsilon}^p = \frac{1}{\eta} \langle \Phi(\sigma) \rangle^n \frac{\partial \Phi(\sigma)}{\partial \sigma} = \frac{3}{2\eta} \langle J(s) - \kappa \rangle^n \frac{s}{J(s)} \tag{2.8}$$

This relationship reflects a flow rule to model viscoplastic behaviour (Perzyna, 1971).

To introduce the influence of damage in the constitutive description, the stress tensor σ in the equations (2.3) and (2.8) is replaced by the effective stress $\sigma/(1-D)$ with D the damage variable (Lemaitre and Chaboche, 1990). The eventual constitutive model then becomes:

$$\varepsilon^e = \varepsilon - \varepsilon^p = \frac{1}{E(1-D)} [(1+\nu)\sigma - \nu\, tr(\sigma) I] \tag{2.9}$$

$$\dot{\varepsilon}^p = \frac{3}{2\eta} \left\langle \frac{J(s)}{1-D} - \kappa \right\rangle^n \frac{s}{J(s)} \tag{2.10}$$

To complete the model equations (2.9) and (2.10) a creep damage evolution law (Kachanov, 1986) is proposed

$$\dot{D} = \left(\frac{J(s)}{K(1-D)} \right)^r \tag{2.11}$$

with K and r positive material constants.

2.2 Uniaxial stress

For a tensile bar with axial stress $\sigma_{11}>0$, the following system of equations is derived from (2.9), (2.10) and (2.11):

$$\varepsilon^e_{11} = \frac{1}{E(1-D)}\sigma_{11} \tag{2.12}$$

$$\dot{\varepsilon}^p_{11} = \frac{1}{\eta}\left\langle \frac{\sigma_{11}}{1-D} - \kappa \right\rangle^n \tag{2.13}$$

$$\dot{D} = \left(\frac{\sigma_{11}}{K(1-D)} \right)^r \tag{2.14}$$

A symbolical representation of this one-dimensional model is displayed in Fig. 1a where $\tilde{\sigma}_{11}=\sigma_{11}/(1-D)$ denotes the effective stress. Fig. 1b shows measured and numerically calculated stress strain diagrams for PS/EPDM bars, produced by pressing at high temperature. The range of strain rates covers the rates occurring in the verification experiment to be discussed in the next section. The material parameters used to fit tensile experiments and simulation results are: E=1.8 10^9 [Pa], κ=1.4 10^7 [Pa], η=8.0 10^{22} [Pa^n s], K=4.2 10^7 [Pa s$^{1/r}$], n=3, r=6. Besides, the value 0.4 will be taken for Poisson's ratio ν.

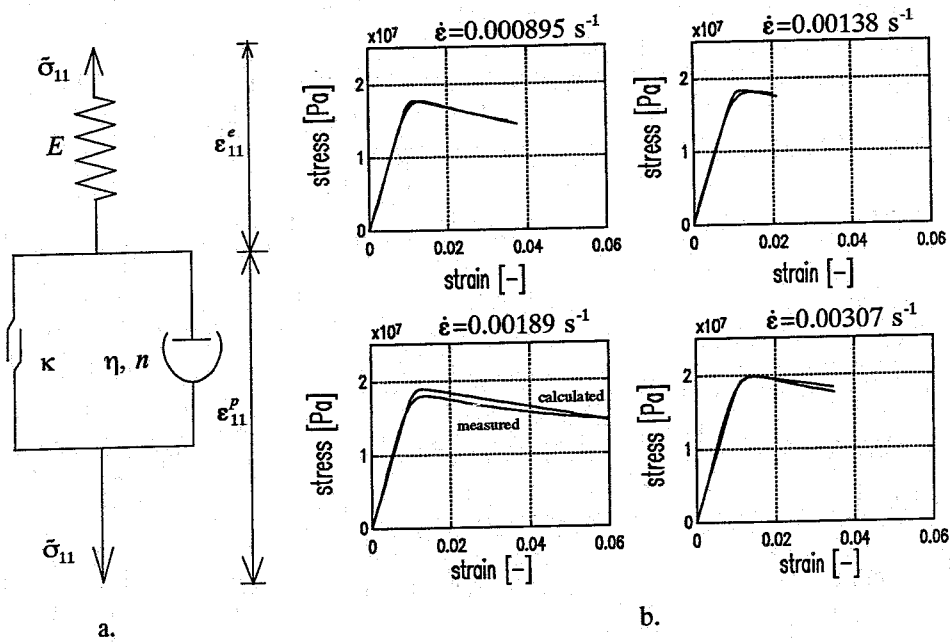

Fig. 1: a. Scheme of the one-dimensional model; b. Calculated and measured stress-strain diagrams at different strain rates.

3. Outline of the experimental verification

To examine the applicability of the constitutive model for the simulation of the behaviour of PS/EPDM in a more complex configuration, a verification experiment has been executed. A tensile test is performed on a thin rectangular (100*150*3 mm^3) plate with a central circular hole (diameter 40 mm). The relative displacement of the upper clamp with respect to the lower clamp is prescribed as a monotonously increasing function of time, relative velocity 0.016 mms^{-1}. In Fig. 2a the experimental set-up is shown. Because of the symmetry only one quarter of the plate is considered in detail. This part is covered with markers, located at the crossings of the dotted lines in Fig. 2a. During the test the positions of the markers are scanned by a camera. The scanning is dynamically executed with the Hentschel random access tracking system (Zamzow, 1990); the measuring time is divided in time-steps of 0.71 s and each step the positions of the markers are recorded by pixel identification. The transformation to real length units is possible by the simultaneous registration of the positions of reference markers.

Inter- and extrapolations of the displacements per time-step enable the determination of the strain distribution. The accuracy of the procedure is limited: the deviations in the components of strain per time-step may be considerable as is demonstrated in Fig. 2b, where the noise in the strains of a particular marker (M, as indicated in Fig. 2a) in the interesting area of the configuration is clearly observable. However, the number of time-steps allows for a reasonable polynomial fit. The measurement was terminated at time-step 106 as complete fracture of the plate occurred.

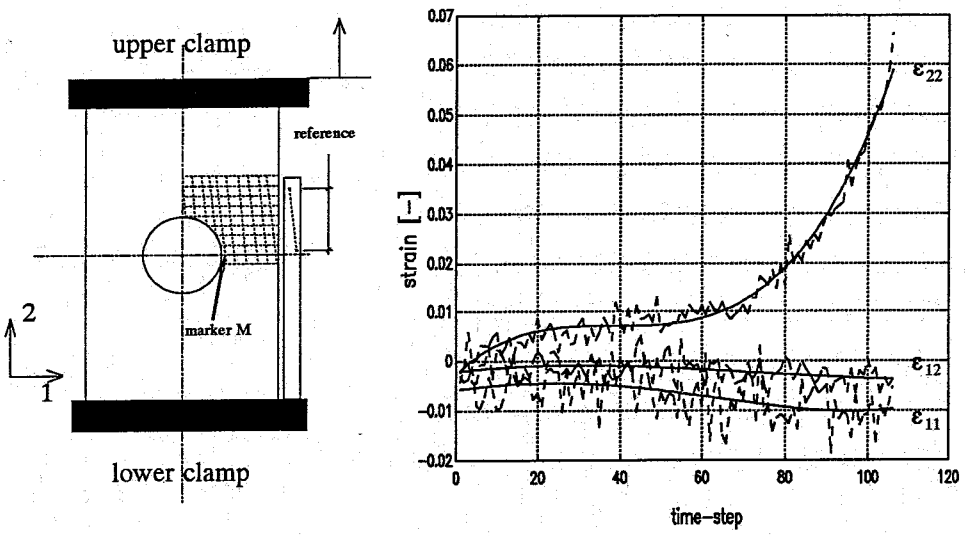

a. b.

Fig. 2: a. Experimental set-up during the test; b. Calculated strains from measured displacements and polynomial fits for marker M.

4. Numerical elaboration

To analyse the mechanical behaviour of arbitrary configurations the finite element method is applied with discretization of the displacement field. To deal with history/time dependence in the constitutive description (2.9), (2.10) and (2.11) the relevant time domain is divided in increments $t_{k-1} \leq t \leq t_k$ (k=1,2,...). For the end of subsequent increments discretized equilibrium is required: the internal nodal forces should balance the external nodal forces. The internal nodal forces after increment k are composed of linear contributions of the stress tensors (σ_k) in the elemental integration points. The calculation of σ_k is performed by an explicit integration scheme, according to

$$\Delta\varepsilon^p = \varepsilon^p_k - \varepsilon^p_{k-1} = \frac{3}{2\eta}\left\langle \frac{J(s_{k-1})}{(1-D_{k-1})} - \kappa \right\rangle^n \frac{s_{k-1}}{J(s_{k-1})}\Delta t \tag{4.1}$$

$$\Delta D = D_k - D_{k-1} = \left(\frac{J(s_{k-1})}{K(1-D_{k-1})} \right)^r \Delta t \tag{4.2}$$

$$\sigma_k = (1-D_{k-1}-\Delta D)\,{}^4H:(\varepsilon_k - \varepsilon^p_{k-1} - \Delta\varepsilon^p) \tag{4.3}$$

with $\Delta t = t_k - t_{k-1}$. Of course, a more sophisticated integration procedure can be pursued, however, the scheme proposed produced sufficiently accurate results. Besides, the above relationships imply that, at increment level, the stress depends linearly on the strain. Consequently, the internal forces are linearly expressed in the nodal displacements. This leads to a standard linear finite element formulation for an incremental step which needs no further explanation.

5. Simulation of the experiment; mesh-refinement

The tensile test on the plate with the circular hole is numerically simulated by the finite element approach. The analysis is evaluated by comparison of measured and calculated strains. Besides, the global stiffness (total tensile force versus clamp displacement) is considered. The simulation is performed for various element meshes to examine the objectivity of the results with respect to mesh-refinement.

5.1 Simulation

To achieve numerical results a quarter of the plate is divided in four node plane stress elements with four integration points. The smallest element (size 5 mm) is located near the point of maximum stress concentration. Along the boundaries of the configuration appropriate kinematical, dynamical and symmetry conditions are prescribed. The simulation is executed in 80 time-increments of 1 s each.

Fig. 3a shows the mesh and the damage developed by the end of the simulation. Figs. 3b and 3c present contourplots of an equivalent strain, here defined by

$$\varepsilon^{eq} = \sqrt{\frac{2}{3}(\varepsilon_{11}^2 + \varepsilon_{22}^2 + 2\varepsilon_{12}^2)} \tag{5.1}$$

derived from computation and experiment, respectively. The distributions of calcula-

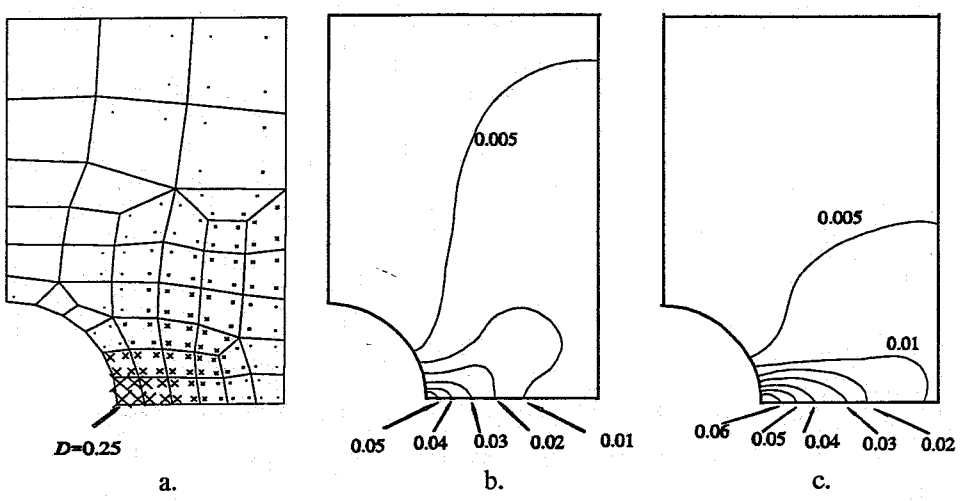

a. b. c.

Fig. 3: a. Accumulation of damage in the final state; b. Calculated equivalent strain; c. Measured equivalent strain.

ted and measured strains are in reasonable agreement. Fig. 4a gives the evolution of the external tensile force (on half the plate) during the incrementation. The post-peak behaviour in the numerical approach is mainly a direct consequence of the introduction of the critical damage concept. From the uniaxial tests, as described in section 2.2, it could be observed that for an average value D equal to 0.25 a complete loss of stiffness (fracture) occurred. This value for D is adopted as the criterion for total local deterioration, which is taken into account by a sudden reduction of the elastic modulus (to 1 % of the original value). The numerous sources of inaccuracy, that might possibly explain the difference between the calculated and measured global response, will not be discussed in this paper.

5.2 Mesh-refinement

The configuration of the plate with circular hole is re-analysed with meshes as displayed in Figs. 4b and 4c. The strain fields and the global response show only minor changes with respect to the results presented before. A slight stiffness reduction can be observed, however, the difference between computation and experiment is certainly not significantly decreased.

6. Conclusion

In this paper an elasto-perfectly-viscoplastic and creep-damageable constitutive description is derived, to model the behaviour of polymer blends, specifically PS/ EPDM. Material parameters, identified by tensile tests at different strain rates, are adequate to simulate the response of a rectangular plate with a circular hole. The calculated strain field appears to be in reasonable agreement with experimental results.

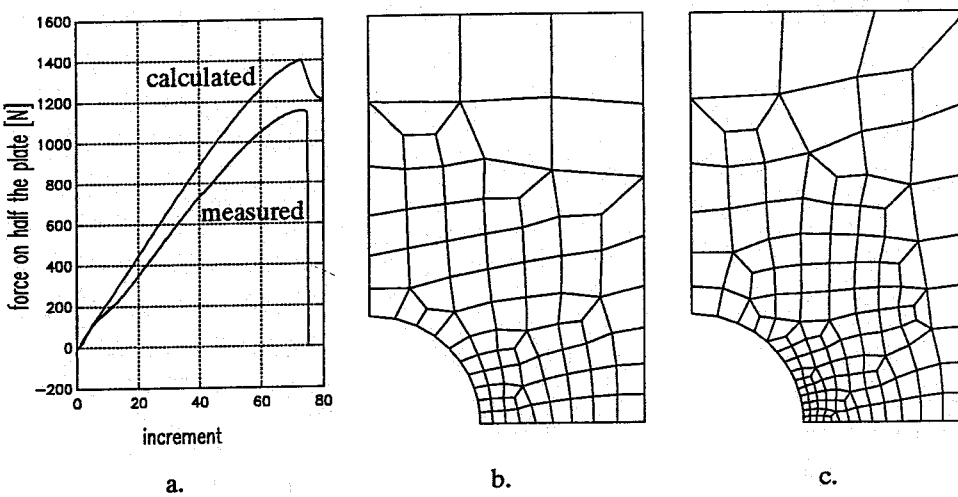

Fig. 4: a. Global response during the incrementation; b. Mesh with smallest element size 2 mm; c. Mesh with smallest element size 1 mm.

The maximum of the calculated force shows to be 20 % larger than the measured value.

The minor effect of mesh-refinement demonstrates that the viscous contribution to the material characterization regularizes the influence of strain softening phenomena: a continuous mesh-refinement leads to converging physically acceptable solutions for damage problems.

References

Kachanov, L.M. (1986) *Introduction to Continuum Damage Mechanics*. Martinus Nijhoff Publishers, Dordrecht.

Lemaitre, J. and Chaboche, J.-L. (1990) *Mechanics of Solid Materials*. Cambridge University Press, Cambridge.

Marquis, D. (1989) Evaluation of material damage due to thermomechanical strain cycles. *Engineering Application of Modern Plasticity. Short course of the Second International Symposium of Plasticity, Nagoya, Japan*, 1-14.

Needleman, A. (1988) Material rate dependence and mesh sensitivity in localization problems. *Comp. Meth. Appl. Mech. Engng.*, **67**, 68-85.

Perzyna, P. (1971) Thermodynamic theory of viscoplasticity. *Advances in Applied Mechanics*, **11**. Academic Press, New York.

Simo, J.C. (1988) Strain softening and dissipation: a unification of approaches. *Cracking and Damage, Strain Localization and Size Effects*, J.Mazars and Z.P.Bazant eds., 440-461. Elsevier Applied Science, London.

Zamzow, H. (1990) The Hentschel random access tracking system HSG 84.30. *Proceedings of the Symposium on Image Based Motion Measurement, La Jolla, California, USA*, J.S.Walton ed., Proceedings of the SPIE (Society of Photo-Optical Instrumentation Engineers) **1356**, 130-133.